JVST B
Journal of Vacuum Science & Technology B

ARTICLE

avs.scitation.org/journal/jvb

Morphologic and electronic changes induced by thermally supported hydrogen cleaning of GaAs (110) facets

Cite as: J. Vac. Sci. Technol. B **41**, 044202 (2023); doi: 10.1116/6.0002733
Submitted: 31 March 2023 · Accepted: 3 May 2023 ·
Published Online: 23 May 2023

View Online

Export Citation

CrossMark

D. S. Rosenzweig,[1,a)] M. Schnedler,[2] R. E. Dunin-Borkowski,[2] Ph. Ebert,[2] and H. Eisele[3]

AFFILIATIONS

[1]Institut für Festkörperphysik, Technische Universität Berlin, 10623 Berlin, Germany
[2]Ernst Ruska-Centrum (ER-C-1) and Peter Grünberg Institut (PGI-5), Forschungszentrum Jülich GmbH, 52425 Jülich, Germany
[3]Institut für Physik, Otto-von-Guericke Universität Magdeburg, 39106 Magdeburg, Germany

Note: This paper is part of the Special Topic Collection: Papers from the 48th Conference on the Physics and Chemistry of Surfaces and Interfaces (PCSI-48) 2023.
[a)]**Electronic mail:** dorothee.rosenzweig@physik.tu-berlin.de

ABSTRACT

Hydrogen exposure and annealing at 400 °C leads to a layer-by-layer etching of the *n*-doped GaAs(110) cleavage surface removing islands and forming preferentially step edge sections with [001] normal vector. In addition, a large density of negatively charged point defects is formed, leading to a Fermi level pinning in the lower part of the bandgap. Their charge transfer level is in line with that of Ga vacancies only, suggesting that adatoms desorb preferentially due to hydrogen bonding and subsequent Ga–H desorption. The results obtained on cleavage surfaces imply that the morphology of nanowire sidewall facets obtained by hydrogen cleaning is that of an etched surface, but not of the initial growth surface. Likewise, the hydrogen-cleaned etched surface does not reveal the intrinsic electronic properties of the initially grown nanowires.

Published under an exclusive license by the AVS. https://doi.org/10.1116/6.0002733

I. INTRODUCTION

III-V nanowires (NWs) attracted much interest due to their unique ability to accommodate lattice mismatched heterostructures without dislocation formation.[1,2] In addition, core-shell structures offer a spatial separation of light absorption and charge carrier drift directions in optoelectronic and photovoltaic applications.[3–6] All applications are, however, affected by the very large surface to volume ratio, which makes an understanding of the surface electronic properties, such as, e.g., Fermi level pinning, and their effect on the underlying layers critical. Therefore, particular interest arose in characterizing the different facets of NWs.[7–20] Due to the large aspect ratio, the dominating facets are the nonpolar side facets, which, hence, govern the surface effects, i.e., electronic properties and growth on side facets. A detailed understanding of the nonpolar side facets during growth is particularly critical for tailoring and optimization of dopant incorporation during the growth of core-shell NW structures. A direct atomically resolved access to the NW side facets during growth proved to be a tremendously difficult task.[21] Hence, NW side facets were rather investigated *ex situ* by STM. For this purpose, the NWs were either As capped and annealed in the ultrahigh vacuum (UHV) system of the STM (Ref. 9) or left uncapped and cleaned by thermally supported hydrogen etching.[7] The critical question is if such prepared side facets have any relation to the original growth surfaces, particularly in terms of defects, morphology, and electronic properties.

Since the investigation of the detailed processes during cleaning directly at the (110) NW side facets is rather difficult, we use equivalent GaAs(110) surfaces obtained by cleavage as the model system, since (110) growth surfaces and cleavage surface exhibit identical surface reconstructions and intrinsic electronic properties. The results obtained on the cleavage surface are then applied to discuss the state of nanowire sidewall facets.

Here, we concentrate on the atomic processes during thermally supported hydrogen etching and their effects on the

Downloaded from http://pubs.aip.org/avs/jvb/article-pdf/doi/10.1116/6.0002733/17790921/044202_1_6.0002733.pdf

Published under an exclusive license by the AVS

morphology, defects, and electronic properties of *n*-doped GaAs (110). We demonstrate experimentally that the hydrogen exposure and annealing leads to a layer-by-layer etching, during which the morphology is governed by the resilience of atoms at specific sites to hydrogen-enhanced desorption. This shows up in the preferential formation of dimer-reconstructed and charge reduced step edges with a [001] normal vector. In addition, Ga vacancies, formed thermally on the enlarged terraces, induce a Fermi level pinning in the lower part of the bandgap. On the basis of these atomic processes observed on the (110) cleavage surface, we conclude that neither the morphology nor the electronic properties of hydrogen-cleaned NW sidewall facets correspond to those of the initial growth facets.

II. EXPERIMENT

For the experiments, we use *n*-type GaAs (001) wafers with Si doping concentrations of nominally $1–2{\times}10^{18}\,\mathrm{cm}^{-3}$. Samples cut from the wafer are cleaved under UHV conditions ($< 2 \times 8^{-8}$ Pa). Cleavage usually yields surfaces with large atomically flat terraces and low densities of steps. However, in order to investigate the effect of hydrogen exposure and annealing on surface morphology and, in particular, on the steps, cleavage surfaces with rather high densities of steps are necessary. As outlined previously, strained GaAs yields upon cleavage macroscopically curvatured (110) cleavage surfaces with high step concentration.[22] Therefore, we strained mechanically in the [001] direction nominally unstrained GaAs to obtain densely stepped surfaces as the model system.

The freshly cleaved GaAs(110) surfaces are exposed to atomic hydrogen, which is provided by a hydrogen atom beam source (HABS) with a cracking efficacy of nominally 98 % (Dr. Eberl MBE-Komponenten GmbH). The hydrogen exposure was performed with a total hydrogen partial pressure of $5{\times}10^{-6}$ Pa and an operation temperature of 1800 °C of the HABS. The hydrogen exposure time of the GaAs(110) surface was chosen to 5 min at 400 °C sample temperature, monitored using a pyrometer. The sample was heated by direct current heating. At the end of the hydrogen exposure, the hydrogen supply is switched off at the same time as the annealing is stopped and the sample is quenched to room temperature. In order to avoid thermal drift in the STM measurements, we waited 2 h for stabilization at room temperature in UHV before starting the STM experiments. All STM measurements were performed at room temperature with electrochemically etched tungsten tips in UHV.

III. RESULTS

A. Surface morphology changes

1. Hydrogen exposure and annealing

Figure 1(a) shows a typical *n*-doped GaAs(110) cleavage surface, consisting of atomically flat terraces separated by predominantly monoatomic steps. The terraces exhibit the well known 1×1 surface relaxation of the GaAs(110) surface.[23] Here, we first focus on the step morphology: In this particular case, we chose a surface with high step density to investigate the hydrogen effect on the step morphology. The cleavage surfaces with high step densities typically exhibit triangular terraces, whose opening angle varies, generally decreasing with step density. In the particular case of Fig. 1(a), the opening angle is very small, resulting in almost parallel steps. The additionally visible nm-sized protrusions are not adsorbates, but rather cleavage defects occurring generally in densely stepped regions.[22,24,25]

Figure 1(b1) reveals the change of the surface morphology of the same cleavage surface shown in (a) after exposure to atomic hydrogen at $400 \pm 20\,^\circ$C for 5 min. The hydrogen exposure results in wider terraces. The few remaining steps exhibit now a preferential orientation along the [$\bar{1}$10] direction. The same experiment on another cleavage surface with triangular terraces with a wider opening angle reveals again the preferential presence of step edges along the [$\bar{1}$10] direction [Fig. 1(b2)]. Note, however, that only step up [$\bar{1}$10]-oriented step edges occur (viewed from left to right). On

Downloaded from http://pubs.aip.org/avs/jvb/article-pdf/doi/10.1116/6.0002733/17790921/044202_1_6.0002733.pdf

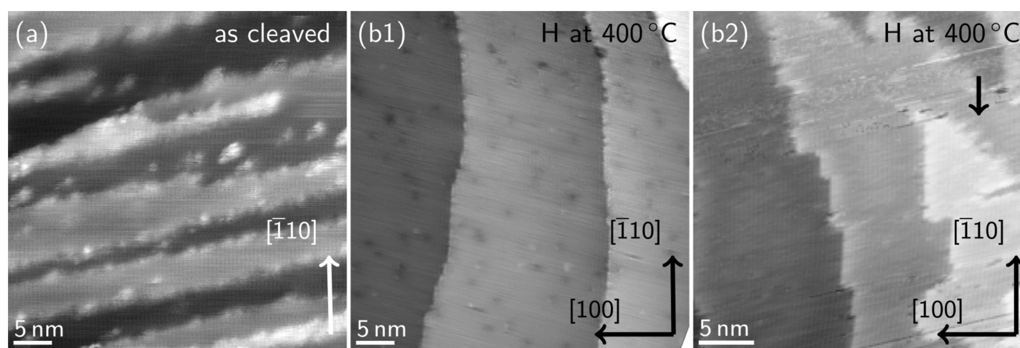

FIG. 1. Effect of hydrogen exposure and simultaneous annealing: (a) Atomically resolved constant-current STM image of the *n*-doped GaAs(110) surface in its as-cleaved state exhibiting a high density of monoatomic steps, acquired at a sample voltage of $V_S = -2.0$ V and tunnel current of $I_T = 30$ pA. (b1) Surface of the same cleavage as (a) after 5 min hydrogen exposure with simultaneous annealing at $400 \pm 20\,^\circ$C, acquired at $V_S = +3.0$ V and $I_T = 50$ pA. The density of steps is considerably lowered and their edges align along the [$\bar{1}$10] direction with [001] normal vector. (b2) A different cleavage surface treated in analogy to (b1) with hydrogen and annealing acquired at $V_S = -2.5$ V and $I_T = 50$ pA. Again, the terraces are delimited with steps exhibiting straight sections with [001] normal vector on the left side, but deep erosion channels on the opposite side (see arrow).

Published under an exclusive license by the AVS

the stepdown side, the step edges exhibit deep perpendicular fjord-like erosion channels (see arrow).

2. Annealing without hydrogen

In order to distinguish the effect of hydrogen exposure from that of only annealing, a freshly cleaved *n*-doped GaAs(110) surface was annealed at the same temperature of $400 \pm 20\,^{\circ}$C without hydrogen exposure as reference experiment. The chosen cleavage surface exhibited again a high density of steps as visible in Fig. 2(a). After 5 min annealing, no detectable change occurred [Fig. 2(b)]. Even after further annealing of 30 min the step edges did not form facets like observed at step edges on the hydrogen-cleaned surface [Fig. 2(c)]. In particular, no straight $[\bar{1}10]$-oriented step edge sections form without hydrogen at the investigated temperature of annealing. The island and step pattern appear rounded and no relation to the underlying crystal symmetry can be discerned.

B. Point defect generation

1. Freshly cleaved surface

The freshly cleaved densely stepped *n*-type GaAs(110) surface without any treatment exhibits primarily missing As dangling bonds as visible in Fig. 2(a). These can be attributed to As vacancies and small vacancy clusters.[26–30] Cleavage-related As vacancy defects were previously observed on *densely stepped* Te- and Si-doped GaAs(110), too.[22,31] The observation of As vacancies on densely stepped *n*-type GaAs(110) surfaces is in contrast to *step-free* surfaces, where only Ga vacancies and adatoms form thermally after cleavage.[32,33]

The formation of different types of vacancies can be traced to the different Fermi level positions on stepped and step-free surfaces: The steps induce a midgap Fermi level pinning,[34] whereas the Fermi level on the step-free surface is close to the conduction band due to the *n*-type doping. Here, we focus in the following on densely stepped surfaces with midgap Fermi level position, where As vacancies dominate.

2. Hydrogen exposed and annealed surface

After hydrogen exposure and simultaneous annealing, a high density of dark depressions can be observed on the newly formed large atomically flat terraces in empty state STM images [Fig. 1(b1)]. These depressions have a diameter of about 2 nm and can be assigned to negative charge centers giving rise each to a local screened Coulomb potential.[35,36] Such negatively charged point defects occur on all step-free regions on *n*-doped GaAs(110) cleavage surfaces and were attributed to Ga surface vacancies.[31–33,37–39] The Ga vacancies are found to form spontaneously even at room temperature.[32,33] The evaluated density of the anticipated Ga vacancies is $4–5\times10^{12}\ \mathrm{cm}^{-2}$.

C. Electronic properties

1. Tunneling spectroscopy

In order to provide a further insight, tunneling spectra were acquired on the hydrogen exposed and annealed surface visible in Fig. 1(b1). The tunnel current is displayed as red symbols on a logarithmic scale in Fig. 3. The current onsets at negative and positive voltages are approximately at −0.7 and +0.8 V. The Fermi level at 0 V is approximately centered within the apparent bandgap, indicating a Fermi level pinning related to the presence of the negatively charged point defects.

2. Extraction of band edge positions

In order to quantify the Fermi level pinning, we simulated the tunnel current following a two-step method:[40,41] First, the charge carrier distributions and the corresponding electrostatic potential of the tungsten tip-vacuum-GaAs semiconductor system in thermal equilibrium are self-consistently derived using finite differences. For this, the doping concentration and density of charged surface defects are taken into account. Second, the tunnel currents through the vacuum barrier are calculated in a WKB approximation–based model using the one-dimensional electrostatic potential along the central axis through the tip apex.[42,43]

Downloaded from http://pubs.aip.org/avs/jvb/article-pdf/doi/10.1116/6.0002733/17790921/044202_1_6.0002733.pdf

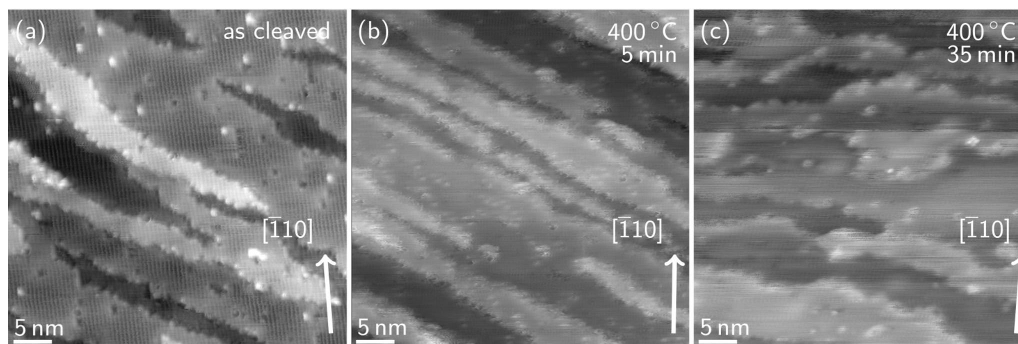

FIG. 2. Effect of heat treatment without hydrogen exposure: (a) Atomically resolved constant-current STM images of the *n*-doped GaAs(110) surface in the as-cleaved state with high density of monoatomic steps, acquired at $V_S = -2.0$ V and $I_T = 50$ pA. (b) Surface of the same cleavage as (a) after 5 min annealing at $400 \pm 20\,^{\circ}$C, acquired at $V_S = -1.8$ V and $I_T = 50$ pA. (c) Surface of the same cleavage as (a) after a total of 35 min annealing at $400 \pm 20\,^{\circ}$C, acquired at $V_S = -1.8$ V and $I_T = 50$ pA.

Published under an exclusive license by the AVS

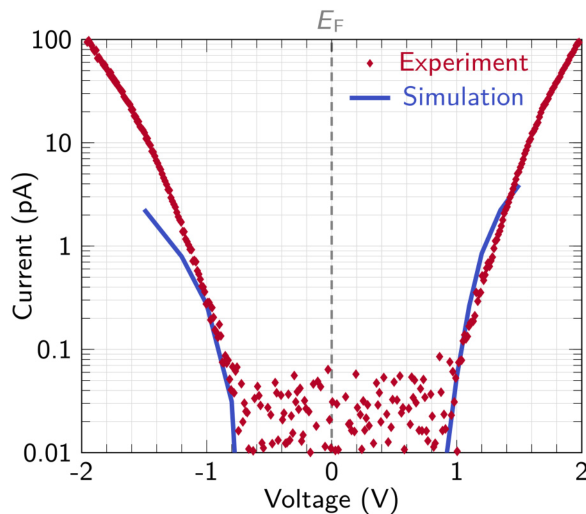

FIG. 3. Tunneling spectrum averaged from 343 individual spectra acquired on the GaAs(110) surface after hydrogen exposure and annealing, shown in Fig. 1(b1). The experimental spectrum (diamond marks) was measured at a tip-sample separation fixed by a set point of $V_{set} = -1.6$ V and $I_{set} = 50$ pA. The solid line illustrates the best fitting simulation of the tunnel current revealing a charge transfer level of the point defects at $E_C - 1.15$ eV.

As parameters, we consider the (i) charge transfer level and (ii) concentration of the charged surface point defects. First, the charge transfer level is modeled as a Gaussian-shaped surface-charge distribution 0.1 eV wide, arising from the convolution of a sharp charge transfer level with the Dirac distribution at room temperature. Second, the density of surface charges is related to the concentration of point defects, extracted from the STM images by directly counting the number of point defect-induced depressions.

The solid line represents the best fitting simulation of the tunnel current obtained for a charge transfer level of $E_C - 1.15$ eV below the conduction band edge and a defect-induced surface charge of 5×10^{12} cm^{-2}. The current at negative (positive) voltages arise from tunneling out of filled valence band states (into empty conduction band states). The upper limit of the charge transfer level can be estimated assuming full pinning to be $E_C - 0.8$ eV, whereas the lower limit is estimated on basis of the uncertainties of the current onsets in the tunnel spectrum and of the defect density to be $E_C - 1.3$ eV.

IV. DISCUSSION

A. Morphology changes due to layer-by-layer hydrogen etching

The experimental results revealed a significant change of the surface morphology after hydrogen exposure and simultaneous annealing. The changes show up in a reduction of the density of steps and a formation of straight sections of the step edges along the $[\bar{1}10]$ direction with [001] normal vector. These morphology changes indicate that the step edges with [001] normal vector are more stable under hydrogen exposure and annealing than all other step directions. This stabilization can be traced back to the formation of a dimer structure at the step edges visible in high resolution STM images,[34] which leads to a reduced charging of the dimer reconstructed step edges as compared with non-reconstructed step edges.[44,45]

Next, we address the relevance of hydrogen exposure for these morphology changes. Annealing without hydrogen at the same temperature does not reduce the step density or create step edges with [001] normal vector even at much longer annealing times as used for the hydrogen exposure. These observations demonstrate that the presence of hydrogen is required for the morphology changes observed.

On this basis, it becomes obvious that hydrogen exposure and annealing at 400 ± 20 °C induces a layer-by-layer etching of the surface: the absence of vacancy islands indicates that hydrogen is not etching the defect free 1×1 terraces primarily, but rather attacks the step edges. Thereby cleavage-induced islandlike terraces delimited by pairs of up and down step edges are removed to expose a surface with reduced step density. The step edges left over are then the most stable step edges, where the hydrogen etching rate is smallest. For n-doped GaAs, the most stable step edge is, thus, the one with [001] normal vector, which exhibits a dimer reconstruction and a reduced charge.[34] The formation of such step edges is also found during sputtering and annealing of GaAs(110) surfaces.[46] The hydrogen-induced appearance of step edges with [001] normal vector is not limited to GaAs(110), but can be observed also at a closer look in STM images of InAs(110) after hydrogen exposure and annealing [see, e.g., apices of terraces in Fig. 2(d) in Ref. 47].

Note that hydrogen exposure without annealing does not lead to a layer-by-layer etching, but rather to point defect generation and local hydrogen adsorption.[48] This outlines the importance of annealing and hence of mobility for activation of layer-by-layer hydrogen etching. Furthermore, there is no indication of hydrogen remaining on the surface after etching, since no local height changes are observed as for local hydrogen adsorption clusters at room temperature.[48]

Without hydrogen, annealing of GaAs(110) under Langmuir conditions leads first to a congruent evaporation, detectable above ~500 °C. Upon further heating above ~600 °C, a decomposition of the surface occurs due to preferential As_2 desorption, as probed by Auger electron spectroscopy and quadrupole mass spectrometry.[49–51] Our experiments in the absence of hydrogen reveal that the congruent evaporation is indeed not yet taking place at 400 ± 20 °C, in line with the previous observations. In contrast, the observation of hydrogen-induced layer-by-layer etching already at such low temperature of 400 ± 20 °C indicates that hydrogen lowers the temperature required for congruent desorption, hence acting as a kind of catalyst.

B. Electronic properties

The analysis of the tunneling spectra in Fig. 3 yielded a defect-induced Fermi level pinning and underlying charge transfer level at $E_C - 1.15^{+0.35}_{-0.15}$ eV below the conduction band edge. This charge transfer level from neutral to negative charge is related to

Downloaded from http://pubs.aip.org/avs/jvb/article-pdf/doi/10.1116/6.0002733/17790921/044202_1_6.0002733.pdf

Published under an exclusive license by the AVS

the presence of the negatively charged surface point defects visible in Fig. 1(b1) and assigned to Ga vacancies.

The here obtained charge transfer level can be compared with charge transfer levels derived from Fermi level position and defect density measurements on comparably Si-doped n-type molecular beam epitaxy (MBE) grown GaAs(110) surfaces. These so-called growth surfaces were prepared after termination of the MBE growth by cooling to room temperature with gradual As_4 flux reduction. STM images reveal that Ga vacancies and unspecified adatoms are present on the such prepared GaAs(110) growth surface.[39] The corresponding x-ray photoelectron spectroscopy (XPS) measurements yielded Fermi level positions in the upper part of the fundamental bandgap between $E_C - 0.4$ and $E_C - 0.55$ eV. On basis of these data, we derived the charge transfer levels for the defects present on three different GaAs(110) growth surfaces using the methodology outlined in the Appendix. The resulting charge transfer levels are shown in Fig. 4 as open diamonds and compared with the charge transfer level obtained here for defects on the hydrogen exposed surface (filled diamond). The charge transfer level of the defects on the growth surfaces is much higher in the bandgap as compared with that obtained on the hydrogen-etched surface.

In order to understand the different Fermi level positions, we turn to density functional calculations of the Ga vacancy on GaAs

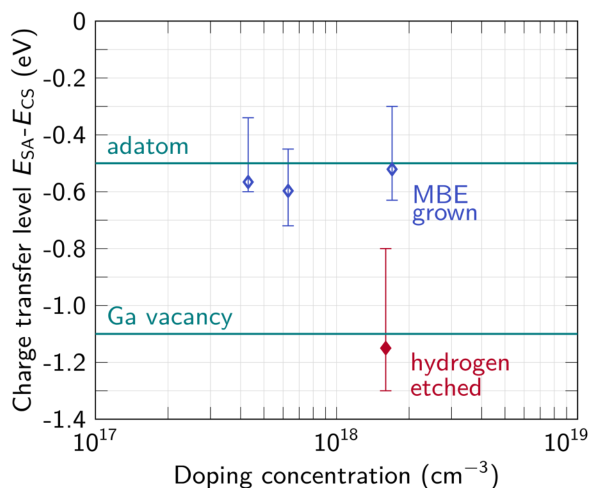

FIG. 4. Comparison of the (0/−) charge transfer level relative to the surface conduction band edge obtained for the defects on the hydrogen-etched Si-doped GaAs(110) surface (filled diamond), extracted from the tunnel current simulation, with those derived from the XPS and STM data of Ishikawa *et al.* (Ref. 39) acquired on the Si-doped GaAs(110) growth surface (empty diamonds). In addition, the horizontal lines indicate the (0/−) charge transfer levels of the Ga vacancy and the Ga adatom, obtained by DFT calculations with LDA approximation (Ref. 28) and corrected for the bandgap underestimation as discussed in the text. The comparison with theory indicates that the measured charge transfer levels on the growth and hydrogen-etched GaAs(110) surfaces arise from different pinning defects: On the growth surface Ga vacancies and adatoms occur, whereas on the hydrogen-etched surface only Ga vacancies remain, attributed to a preferential etching of adatoms by hydrogen.

(110).[28] The theory yields a negative charge for Ga vacancies on n-type GaAs(110) surfaces, changing to neutral for a Fermi level position of 0.3 eV above the valence band. Considering the underestimation of the fundamental bandgap in the density functional theory (DFT) with local density approximation (LDA), the (0/−) charge transfer level could be somewhat higher in energy. However, the density of states of the defect level has a spatial distribution overlapping largely with that of the filled As dangling bond. This suggests that the defect level is predominantly derived from valence band states and, hence, the correction of the bandgap (quasiparticle corrections) would not result in a significant shift relative to the valence band edge. Following this, the calculated (0/−) charge transition level of Ga vacancies is at $E_C - 1.1$ eV. This value fits well to the here measured Fermi level position on hydrogen-etched and annealed GaAs(110) surfaces but is too low for the observed Fermi level positions on the n-type GaAs(110) growth surface.[39]

For understanding the Fermi level position on the growth surface, we recall that all intrinsic point defects on the GaAs(110) surface (i.e., Ga vacancy, As vacancy, antisite defect, As adatom, interstitial atoms) except the Ga adatom have only (0/−) charge transfer levels in the lower part of the fundamental bandgap.[28] The Ga adatom exhibits two energetically almost equal bonding sites,[52] of which one has a (0/−) charge transfer level in the upper part of the fundamental bandgap.[28] The calculated position of the uppermost (0/−) charge transition level for Ga adatoms is 0.7 eV above the valence band with a bandgap underestimation of ∼0.4 eV.[28] Considering that the defect state has no clear valence or conduction band-derived density of states, we assume that the bandgap (quasiparticle) correction can be approximated by a shift of 0.2 eV toward the conduction band, yielding a value of $E_C - 0.5$ eV below the conduction band. This calculated value for the (0/−) charge transfer level of the Ga adatom fits well to the Fermi level positions measured by XPS and the derived charge transfer levels for defects on the n-type GaAs(110) growth surfaces. Hence, we anticipate that adatoms govern the Fermi level pinning on the growth surfaces.

The presence of adatoms on the growth surface is corroborated on the one hand by the STM images.[39] On the other hand, Ga vacancies are known to form spontaneously on step-free n-doped GaAs(110) surfaces, creating Ga adatoms, whose presence can be detected in STM images.[33] The presence of Ga adatoms is related to their large bonding energy of 2 eV,[53] effectively suppressing desorption. Therefore, the Fermi level positions on the growth surfaces can be attributed to the copresence of Ga adatoms and vacancies.

For the hydrogen-etched surface, the agreement of the measured charge transfer level with that calculated for Ga vacancies suggests that only Ga vacancies are present. This is conceivable, since individual Ga adatoms represent preferred bonding sites for hydrogen atoms, followed by Ga–H molecular desorption. Thus, no adatoms are expected to remain on the hydrogen-etched surface.

C. Application to nanowire facets

The observations presented above have some critical implications on the interpretation and understanding of the morphology

Downloaded from http://pubs.aip.org/avs/jvb/article-pdf/doi/10.1116/6.0002733/17790921/044202_1_6.0002733.pdf

Published under an exclusive license by the AVS

and electronic properties of NW sidewall facets, previously observed in STM images.[12,16,19] First, we address the morphology. As outlined above, the hydrogen cleaning procedure results in a layer-by-layer etching, in which the surface morphology is governed by the resilience in the face of hydrogen-enhanced removal of atoms. This results in *n*-type zincblende (110) sidewall facets in terraces separated by steps with edge segments aligned preferentially along the [$\bar{1}$10] direction. Indeed, these types of step edge orientations can be observed on the sidewalls facets of zincblende segments of InAs[16] and InP NWs.[54] Thus, the surfaces of NWs cleaned by hydrogen etching do not represent growth surfaces, but rather etch surfaces.

Simultaneously, the electronic structure measured on hydrogen-cleaned surfaces does not necessarily reveal the intrinsic electronic structure of the NW bulk. As illustrated above, the Fermi level position at the hydrogen-etched *n*-doped GaAs(110) surface is governed by thermally formed Ga vacancies. We anticipate that for *p*-type III-V(110) surfaces thermally formed group V vacancies pin the Fermi level.[55–57] Thus, the Fermi level position of hydrogen-cleaned NW facets is not governed by doping, but rather defined by the cleaning procedure and thermal treatment during/after it.

Furthermore, for NWs grown with Au droplets as catalyst, it was shown that the Au redistributes in small clusters over the NW sidewall facets upon annealing.[19] Hence, the Au would govern the surface pinning in those cases with a Fermi level position 0.4 eV above the valence band as found for Au on GaAs(110) cleavage surfaces.[58] This is in good agreement with the Fermi level position visible in tunneling spectra acquired on (110) sidewall facets of GaAs NWs grown with Au catalyst and cleaned with hydrogen etching and annealing.[11,59] Hence, the electronic properties, namely, the Fermi level position, of hydrogen-cleaned surfaces do in most cases not reveal the intrinsic properties of the underlying NW material, with possible repercussions on prior band offset determinations.[11]

In this context, it is noteworthy to recall that a planar molecular beam epitaxy growth surface, mentioned above solely for comparison purposes with the hydrogen-etched surface, is not necessarily equal to the NW growth facet: The planar GaAs(110) growth surfaces[39] are grown by molecular beam epitaxy under group V-rich conditions. The group V-rich growth conditions are close to the thermodynamical equilibrium conditions and lead to rather stoichiometric GaAs(110) surfaces. In contrast, NW growth is typically undertaken with much lower group V-III supply ratio resulting in growth under Ga-rich conditions.[60] It can be anticipated that this leads to large concentrations of Ga adatoms at the sidewall surfaces during actual synthesis. These Ga adatoms can be expected to pin the Fermi level position of NW growth surfaces in the upper part of the fundamental bandgap. This Fermi level position is distinctively different from the Ga vacancy governed pinning level of hydrogen-etched surfaces in the lower part of the bandgap. The presence of different Fermi level positions during planar and NW growth can be anticipated to result in different dopant incorporation, too.

Since hydrogen cleaning changes the morphology and electronic properties of the GaAs(110) surface (in a unique manner), one could believe that the alternative arsenic capping for protection against oxidation followed by thermal decapping in the UHV characterization system is a better choice. However, even this approach has been shown to induce surface As antisite defects and island nucleation during arsenic decapping.[19,61] Hence, in order to access the NW growth surface, it is a prerequisite to transfer the as-grown NWs under UHV into the STM.

V. CONCLUSION

Hydrogen exposure and annealing at 400 °C leads to a layer-by-layer etching of the *n*-doped GaAs(110) cleavage surface. The etching acts preferentially at step edges removing islands, thereby reducing the density of steps considerably. Simultaneously, steps form edge sections with [001] normal vector. Their uncharged dimer reconstruction is anticipated to lead to higher stability against hydrogen-induced desorption of atoms as compared to all other charged step orientations. The hydrogen exposure does not create vacancy islands. In addition, the hydrogen etched cleavage surfaces exhibit a large density of negatively charged point defects. Their charge transfer level derived from the Fermi level pinning is in the lower part of the bandgap, in contrast to MBE grown surfaces, where the pinning and charge transfer level is in the upper part of the bandgap. This is attributed to the presence of Ga adatoms in addition to Ga vacancies on the growth surfaces, whereas on hydrogen-etched surfaces no adatoms remain due to the preferential hydrogen bonding to Ga adatoms and subsequent Ga–H desorption.

The results obtained on (110) cleavage surfaces as model system demonstrate that hydrogen cleaning of NW (110) sidewall facets exposed after growth to air will not result in a surface morphology corresponding to the initial growth facet, but rather yield a layer-by-layer etched surface morphology. The intrinsic electronic properties of the growth facets are not probed due to the formation of charged surface defects during hydrogen cleaning. The properties of hydrogen cleaned (10$\bar{1}$0) and (11$\bar{2}$0) sidewall facets of NW wurtzite structure segments need to be interpreted with similar caution. Hence, the only access to NW growth facets and their intrinsic electronic properties is the *in situ* investigation without interruption of the UHV using STM.

Downloaded from http://pubs.aip.org/avs/jvb/article-pdf/doi/10.1116/6.0002733/17790921/044202_1_6.0002733.pdf

ACKNOWLEDGMENTS

The authors acknowledge the Deutsche Forschungsgemeinschaft (DFG, German Research Foundation) (Project No. 390247238) for financial support. The authors thank M. Hjort, A. Mikkelsen, and R. Timm for fruitful discussions. They also thank M. N. L. Hansemann and W. Martyanov for experimental support.

AUTHOR DECLARATIONS

Conflict of Interest

The authors have no conflicts to disclose.

Author Contributions

D. S. Rosenzweig: Conceptualization (equal); Data curation (equal); Investigation (equal); Visualization (equal); Writing – original draft (equal); Writing – review & editing (equal).

Published under an exclusive license by the AVS

M. Schnedler: Data curation (equal); Writing – original draft (equal); Writing – review & editing (equal). **R. E. Dunin-Borkowski:** Supervision (equal). **Ph. Ebert:** Conceptualization (equal); Data curation (equal); Funding acquisition (equal); Project administration (equal); Writing – original draft (equal); Writing – review & editing (equal). **H. Eisele:** Conceptualization (equal); Funding acquisition (equal); Project administration (equal); Supervision (lead); Writing – review & editing (equal).

DATA AVAILABILITY

The data that support the findings of this study are available from the corresponding author upon reasonable request.

APPENDIX: DERIVATION OF CHARGE TRANSFER LEVELS

1. Theory

The presence of charged defects at a semiconductor surface induces a screening by a space charge region near/below the surface of the underlying bulk semiconductor. In equilibrium, the modulus of the surface charge density of the defects Q_{SS} and the accumulated charge density within the space charge region Q_{SC} are equal, but due to the charge neutrality condition both charge densities have the opposite sign, i.e.,[62]

$$Q_{SS} + Q_{SC} = 0. \tag{A1}$$

The surface charge density is given by the density of surface defects n_{SA}, the charge transfer level E_{SA} of the defects, and the position of the Fermi level E_F by[62]

$$Q_{SS} = \frac{-en_{SA}}{e^{\frac{E_{SA}-E_F}{kT}} + 1}. \tag{A2}$$

The minus sign in the numerator is due to the negative charge of the surface defects (acceptors) in our case. The energy difference of the charge transfer level and the Fermi level $E_{SA} - E_F$ is given by

$$E_{SA} - E_F = (E_{SA} - E_{CS}) - (E_C - E_{CS}) + (E_C - E_F). \tag{A3}$$

E_C and E_{CS} are the positions of the conduction band in the bulk and at the surface, respectively). $E_{CS} - E_C$ is the band bending eV_s at the surface, which is extracted from the measurement of the position of the Fermi level relative to the surface conduction band edge $E_{CS} - E_F$ by photoelectron spectroscopy or STS.

The charge density of the space charge region is given by[62]

$$Q_{SC} = \sqrt{2\epsilon_0\epsilon_r n_{dop} kT\left[\exp\left(-\left|\frac{eV_s}{kT}\right|\right) + \left|\frac{eV_s}{kT}\right| - 1\right]}, \tag{A4}$$

with n_{dop} being the donor doping concentration.

This yields for the charge transfer level relative to the surface conduction band edge

$$E_{SA} - E_{CS} = kT \cdot \ln\left(\frac{en_{SA}}{\sqrt{2\epsilon_0\epsilon_r n_{dop} kT\left[\exp(-|\frac{eV_s}{kT}|) + |\frac{eV_s}{kT}| - 1\right]}} - 1\right) + (E_C - E_{CS}) - (E_C - E_F). \tag{A5}$$

The energy difference between the Fermi energy and the conduction band edge in the bulk has been determined from the charge neutrality condition.

2. Experimental procedure

We apply the above equations to the combined XPS and STM data obtained for Si-doped GaAs(110) growth surfaces by Ishikawa *et al.*,[39] as a reference to the here determined charge transfer level on hydrogen-etched GaAs(110). The Fermi level position relative to the surface conduction band edge is extracted either from XPS data, whereas the density of negatively charged surface defects is derived by counting the individual defects in STM images.

In addition, the doping concentration needs to be known. In our case, we used the specification of the GaAs wafers used for the cleavage samples. In case of the work of Ishikawa *et al.*, the free electron concentration was probed by *C-V* measurements on an Au-GaAs(110) Schottky contact, fabricated after the termination of the STM/XPS measurements. Since the GaAs(110) surfaces exhibit a upward band bending, the measured net charge corresponds to the net concentration of Si donors in the material. The charge transfer levels given in Fig. 4 are determined on basis of the here described methodology.

As side note, the differences of the net Si donor concentration achieved by MBE growth between layers grown on (001) and (110) surfaces can be attributed to the different band bending present at the growth surfaces: The polar *n*-doped GaAs(001) surface always exhibits an upward band bending due to the midgap pinning induced by the surface states of the 2×4 reconstruction. In contrast, the defect free nonpolar GaAs(110) surface exhibits flatband conditions. Next, we consider the self-compensation effect of Si in GaAs: Si incorporates on both Ga and As lattice sites, yielding donors and acceptors, respectively. With increasing doping (and, thus, increasing Fermi level position), the compensation by Si_{As} and Si clusters increases, reducing the incorporation as donors.[32] This is corroborated by DFT calculations, which show a lower formation energy for Si donors than Si acceptors for *p*-type material and a reversal for high *n*-doped material.[63,64] Hence, during growth of GaAs(001) with midgap pinning at the growth surface, all Si atoms are incorporated as donors. However, during growth on unpinned, hence *n*-type GaAs(110), Si atoms exhibit a partial incorporation on As sites as acceptors and in uncharged Si clusters. As a result, a 5×10^{18} cm^{-3} Si concentration yields approximately 1.4×10^{18} cm^{-3} Si atoms in Si clusters and 0.8×10^{18} cm^{-3} Si atoms on As lattice sites (derived by interpolation from Domke *et al.*[32]). Thus, the effective net Si donor concentration is reduced to 2×10^{18} cm^{-3}. This is in very good agreement with the values reported by Ishikawa *et al.*[39] This corroborates that taking the

Downloaded from http://pubs.aip.org/avs/jvb/article-pdf/doi/10.1116/6.0002733/17790921/044202_1_6.0002733.pdf

Published under an exclusive license by the AVS

electron concentrations as measured using the Schottky contacts by Ishikawa *et al.* as net Si donor concentrations is meaningful for the determination of the charge transfer level relative to the conduction band edge at the surface.

REFERENCES

[1]H. J. Joyce, Q. Gao, H. H. Tan, C. Jagadish, Y. Kim, X. Zhang, Y. Guo, and J. Zou, Nano Lett. **7**, 921 (2007).
[2]B. A. Wacaser, K. Deppert, L. S. Karlsson, L. Samuelson, and W. Seifert, J. Cryst. Growth **287**, 504 (2006).
[3]B. Mayer *et al.*, Nat. Commun. **4**, 2931 (2013).
[4]S. Breuer, C. Pfuller, T. Flissikowski, O. Brandt, H. T. Grahn, L. Geelhaar, and H. Riechert, Nano Lett. **11**, 1276 (2011).
[5]G. Mariani, A. C. Scofield, C.-H. Hung, and D. L. Huffaker, Nat. Commun. **4**, 1497 (2013).
[6]L. C. Chuang, F. G. Sedgwick, R. Chen, W. S. Ko, M. Moewe, K. W. Ng, T.-T. D. Tran, and C. Chang-Hasnain, Nano Lett. **11**, 385 (2011).
[7]E. Hilner, U. Håkanson, L. E. Fröberg, M. Karlsson, P. Kratzer, E. Lundgren, L. Samuelson, and A. Mikkelsen, Nano Lett. **8**, 3978 (2008).
[8]T. Xu, J. P. Nys, A. Addad, O. I. Lebedev, A. Urbieta, B. Salhi, M. Berthe, B. Grandidier, and D. Stiévenard, Phys. Rev. B **81**, 115403 (2010).
[9]T. Xu *et al.*, Nanotechnology **23**, 095702 (2012).
[10]P. Capiod *et al.*, Appl. Phys. Lett. **103**, 122104 (2013).
[11]M. Hjort, S. Lehmann, J. Knutsson, R. Timm, D. Jacobsson, E. Lundgren, K. Dick, and A. Mikkelsen, Nano Lett. **13**, 4492 (2013).
[12]M. Hjort *et al.*, ACS Nano **8**, 12346 (2014).
[13]A. D. Álvarez *et al.*, Nano Lett. **15**, 6440 (2015).
[14]J. L. Webb, J. Knutsson, M. Hjort, S. Gorji Ghalamestani, K. A. Dick, R. Timm, and A. Mikkelsen, Nano Lett. **15**, 4865 (2015).
[15]T. Xu *et al.*, Appl. Phys. Lett. **107**, 112102 (2015).
[16]J. V. Knutsson, S. Lehmann, M. Hjort, P. Reinke, E. Lundgren, K. A. Dick, R. Timm, and A. Mikkelsen, ACS Appl. Mat. Interfaces **7**, 5748 (2015).
[17]M. Schnedler *et al.*, Phys. Rev. B **94**, 195306 (2016).
[18]M. Hjort, P. Kratzer, S. Lehmann, S. J. Patel, K. A. Dick, C. J. Palmstrøm, R. Timm, and A. Mikkelsen, Nano Lett. **17**, 3634 (2017).
[19]A. D. Álvarez *et al.*, Nanotechnology **30**, 324002 (2019).
[20]M. Schnedler *et al.*, Nano Lett. **19**, 8801 (2019).
[21]F. M. Ross, Rep. Prog. Phys. **73**, 114501 (2010).
[22]P. Quadbeck, Ph. Ebert, K. Urban, J. Gebauer, and R. Krause-Rehberg, Appl. Phys. Lett. **76**, 300 (2000).
[23]R. M. Feenstra, J. A. Stroscio, J. Tersoff, and A. P. Fein, Phys. Rev. Lett. **58**, 1192 (1987).
[24]M. A. Rosentreter, M. Wenderoth, N. H. Theuerkrauf, A. J. Heinrich, M. A. Schneider, and R. G. Ulbrich, Phys. Rev. B **56**, 10538 (1997).
[25]K. Sauthoff, M. Wenderoth, A. J. Heinrich, M. A. Rosentreter, K. J. Engel, T. C. G. Reusch, and R. G. Ulbrich, Phys. Rev. B **60**, 4789 (1999).
[26]G. Lengel, R. Wilkins, G. Brown, M. Weimer, J. Gryko, and R. E. Allen, Phys. Rev. Lett. **72**, 836 (1994).
[27]Ph. Ebert, K. Urban, and M. G. Lagally, Phys. Rev. Lett. **72**, 840 (1994).
[28]G. Schwarz, "Untersuchungen zu Defekten auf und nahe der (110)-Oberfläche von GaAs und weiteren III-V-Halbleitern," Ph.D. thesis (Technische Universität Berlin, Berlin, 2002).
[29]Ph. Ebert, Surf. Sci. Reports **33**, 121 (1999).
[30]L. J. Whitman, J. A. Stroscio, R. A. Dragoset, and R. J. Celotta, Phys. Rev. B **42**, 7288 (1990).
[31]G. Cox, K. Graf, D. Szynka, U. Poppe, and K. Urban, Vacuum **41**, 591 (1990).
[32]C. Domke, Ph. Ebert, M. Heinrich, and K. Urban, Phys. Rev. B **54**, 10288 (1996).
[33]S. Landrock, "Investigation of nanoscale potential fluctuations and defects in 2D semiconducting structures by scanning tunneling microscopy," Ph.D. thesis (RWTH Aachen, Juel-4290, Forschungszentrum Jülich, 2009).
[34]S. Gaan, R. M. Feenstra, Ph. Ebert, R. E. Dunin-Borkowski, J. Walker, and E. Towe, Surf. Sci. **606**, 28 (2012).
[35]J. A. Stroscio, R. M. Feenstra, and A. P. Fein, Phys. Rev. Lett. **58**, 1668 (1987).
[36]R. J. Hamers, J. Vac. Sci. Technol. B **6**, 1462 (1988).
[37]G. Lengel, R. Wilkins, G. Brown, and M. Weimer, J. Vac. Sci. Technol. B **11**, 1472 (1993).
[38]G. Lengel, R. Wilkins, M. Weimer, J. Gryko, and R. Allen, in *22nd International Conference on the Physics of Semiconductors*, edited by D. Lockwood (World Scientific, Singapore, 1995), Vol. 1, pp. 479–484.
[39]Y. Ishikawa, N. Tsurumi, T. Fukui, and H. Hasegawa, J. Vac. Sci. Technol. B **16**, 2387 (1998).
[40]M. Schnedler, V. Portz, P. H. Weidlich, R. E. Dunin-Borkowski, and Ph. Ebert, Phys. Rev. B **91**, 235305 (2015).
[41]M. Schnedler, R. E. Dunin-Borkowski, and Ph. Ebert, Phys. Rev. B **93**, 195444 (2016).
[42]J. Bono and R. H. Good, Surf. Sci. **175**, 415 (1986).
[43]R. M. Feenstra and J. A. Stroscio, J. Vac. Sci. Technol. B **5**, 923 (1987).
[44]M. Heinrich, C. Domke, Ph. Ebert, and K. Urban, Phys. Rev. B **53**, 10894 (1996).
[45]M. Heinrich, "Mechanismen der Desorption und Entmischung auf Indiumphosphid (110)-Oberflächen bei thermischer Behandlung," Ph.D. thesis (RWTH Aachen, Juel-3385, Forschungszentrum Jülich, 1997).
[46]R. J. Pechman, X.-S. Wang, and J. H. Weaver, Phys. Rev. B **51**, 10929 (1995).
[47]M. Hjort, J. V. Knutsson, B. Mandl, K. Deppert, E. Lundgren, R. Timm, and A. Mikkelsen, Nanoscale **7**, 9998 (2015).
[48]D. S. Rosenzweig, M. N. L. Hansemann, M. Schnedler, Ph. Ebert, and H. Eisele, Phys. Rev. Mater. **6**, 124603 (2022).
[49]C. T. Foxon, B. A. Joyce, R. F. C. Farrow, and R. M. Griffiths, J. Phys. D: Appl. Phys. **7**, 2422 (1974).
[50]B. Goldstein, D. J. Szostak, and V. S. Ban, Surf. Sci. **57**, 733 (1976).
[51]F. Proix, A. Akremi, and Z. T. Zhong, J. Phys. C: Solid State Phys. **16**, 5449 (1983).
[52]S. Kaku and J. Yoshino, Small **16**, 2002296 (2020).
[53]J. N. Shapiro, A. Lin, D. L. Huffaker, and C. Ratsch, Phys. Rev. B **84**, 085322 (2011).
[54]S. R. McKibbin *et al.*, Nano Lett. **20**, 887 (2020).
[55]Ph. Ebert, M. Heinrich, M. Simon, K. Urban, and M. G. Lagally, Phys. Rev. B **51**, 9696 (1995).
[56]Ph. Ebert, K. Urban, L. Aballe, C. H. Chen, K. Horn, G. Schwarz, J. Neugebauer, and M. Scheffler, Phys. Rev. Lett. **84**, 5816 (2000).
[57]U. Semmler, M. Simon, Ph. Ebert, and K. Urban, J. Chem. Phys. **114**, 445 (2001).
[58]R. M. Feenstra, Phys. Rev. Lett. **63**, 1412 (1989).
[59]The band edge positions are determined erroneously from tunneling spectra in Ref. 11 by assuming no pinning through defects and, thus, a large tip-induced band bending. However, a logarithmic display of the same tunnel current data corrected for the used ramp in tip-sample separation reveals a valence band current onset at −0.4 V, a defect current at small positive voltages and a conduction band current onset at +1 V, hence yielding a correct bandgap and indicating rather a full pinning.
[60]K. A. Dick, P. Caroff, J. Bolinsson, M. E. Messing, J. Johansson, K. Deppert, L. R. Wallenberg, and L. Samuelson, Semicond. Sci. Technol. **25**, 024009 (2010).
[61]Ph. Ebert, C. Domke, and K. Urban, Appl. Phys. Lett. **78**, 480 (2001).
[62]W. Mönch, *Semiconductor Surfaces and Interfaces*, 3rd ed. (Springer, Berlin, 2001).
[63]R. W. Jansen and O. F. Sankey, Phys. Rev. B **39**, 3192 (1989).
[64]J. E. Northrup and S. B. Zhang, Phys. Rev. B **47**, 6791 (1993).

Downloaded from http://pubs.aip.org/avs/jvb/article-pdf/doi/10.1116/6.0002733/17790921/044202_1_6.0002733.pdf

Published under an exclusive license by the AVS